Comparing Two Contrail Models Under Certain and Uncertain Inputs

Caleb Akhtar Martínez* and Jerome P. Jarrett†
University of Cambridge, Cambridge, CB2 1PZ, England, United Kingdom

There is evidence suggesting that condensation trails (contrails) are at least as warming as carbon dioxide for aviation. Contrail warming effects can be reduced with contrail avoidance strategies. A key element necessary to develop effective contrail avoidance techniques are contrail models. Such models require speed to be implemented into dispatcher workflow, and a minimum accuracy to ensure a net environmental benefit. No models have been proven to be suitable yet. To understand the capabilities of current models, two existing models of different fidelities, CoCiP and APCEMM, are compared in this investigation under certain and uncertain inputs. The comparison of the models under uncertainty is necessary to determine the model sensitivity at different timescales. Further, propagating uncertainties is required for their primary use case since weather data are highly uncertain. The findings presented reveal that the models display similar behaviors when varying the relative humidity and ambient temperature, but they otherwise disagree in the evolution of the contrail properties with time. An increased amount of appropriate validation data is necessary to create a model suitable for real-life contrail avoidance. This investigation also estimated the minimum accuracy required for a contrail avoidance model to be ~65 %.

I. Nomenclature

α	=	Contrail ice mass per unit length
η_{ov}	=	Overall efficiency of the aircraft
θ	=	A random event
Λ	=	Model accuracy
ρ_{atm}	=	Ambient air density
ξ	=	The germ of the Polynomial Chaos Expansion of a random variable
ξ_i^*	=	i-th sample of ξ
σ	=	Standard deviation
Φ_j	=	j-th orthogonal polynomial in the Polynomial Chaos Expansion of a random variable
$\mathbf{A}$	=	The matrix containing the basis orthogonal polynomials evaluated at each sampled germ ξ_i^*
$\mathbf{b}$	=	The vector containing the sample outputs of the deterministic model evaluated at the corresponding ξ_i^*
c_p^{air}	=	Isobaric specific heat of air
$\text{EI}_{\text{H}_2\text{O}}$	=	Water Emissions Index
$F(X)$	=	Cumulative Density Function of X
FNR	=	False Negative Rate
FPR	=	False Positive Rate
$f(\xi)$	=	A function of ξ
$G(\xi)$	=	Cumulative Density Function of ξ
$g(\xi)$	=	A function of ξ
$h(u)$	=	Inverse Cumulative Density function of X
I	=	Contrail ice mass mixing ratio
$K(\theta)$	=	A random parameter
K_i^*	=	i-th sample of K
k_j	=	j-th deterministic coefficient in the Polynomial Chaos Expansion of the random parameter K

*Ph.D. Candidate, Department of Engineering, ca525@cam.ac.uk
†University Senior Lecturer, Department of Engineering, Senior Member AIAA.

$l(u)$	=	Inverse Cumulative Density function of ξ
M_{ratio}	=	Ratio of molar masses of dry air and water vapor
m	=	Gradient of the mixing line in a p-T chart
N	=	Number of samples
P	=	Maximum order of the Polynomial Chaos Expansion
p_V	=	Water vapor pressure
p_{atm}	=	Ambient pressure
$p_{\text{sat}}^{\text{ice}}$	=	Vapor pressure at ice saturation
$p_{\text{sat}}^{\text{liq}}$	=	Vapor pressure at water saturation
Q_{fuel}	=	Lower Heating Value of the fuel
RF	=	Radiative forcing
RF_{AIC}	=	Radiative forcing due to AIC
RF_{CO_2}	=	Radiative forcing due to carbon dioxide
RF_{LW}	=	The component of the outgoing LW radiation reflected by the contrail
RF_{SW}	=	The component of the incoming SW radiation reflected by the contrail
RH_{liq}	=	Relative humidity with respect to water saturation
RH_{ice}	=	Relative humidity with respect to ice saturation
RH_{LC}	=	Critical relative humidity with respect to water saturation for contrail formation
S	=	Contrail cross-sectional area
T	=	Temperature
T_{atm}	=	Ambient temperature
T_{LM}	=	Critical temperature for contrail formation
TNR	=	True Negative Rate
TPR	=	True Positive Rate
t	=	Time
u	=	A random variable uniformly distributed between 0 and 1
$W(\xi)$	=	Probability Density Function of ξ
$X(\theta)$	=	A random variable
$\mathbf{x}$	=	The vector containing the unknown coefficients of the spectral expansion of Y
x_j	=	j-th deterministic coefficient in the Polynomial Chaos Expansion of the random variable X
$Y(\theta)$	=	A random variable
Y_i^*	=	i-th sample of Y
y_j	=	j-th deterministic coefficient in the Polynomial Chaos Expansion of the random variable Y
AIC	=	Aviation-Induced Cloudiness
APCEMM	=	Aircraft Plume Chemistry, Emissions, and Microphysics Model
CDF	=	Cumulative Density Function
CoCiP	=	Contrail Cirrus Prediction model
I-PCE	=	Intrusive Polynomial Chaos Expansion
LOSU	=	Level of Scientific Understanding
LW	=	Long-Wave
MC	=	Monte Carlo
NI-PCE	=	Non-Intrusive Polynomial Chaos Expansion
PCE	=	Polynomial Chaos Expansion
PDF	=	Probability Density Function
SW	=	Short-Wave

II. Introduction

Aviation CO_2 emissions are 2.5 % of current anthropogenic CO_2 emissions, and have risen over the past eighty years [1]. Maintaining such growth rate would soon make aviation one of the leading polluters globally. With the path to net-zero CO_2 emissions becoming clearer, non-CO_2 warming effects, including condensation trails (contrails), are becoming increasingly important.

The mechanism via which global warming occurs is the greenhouse effect, making anthropogenic clouds likely contributors to global warming. In 2013 contrails had an estimated instantaneous warming of 50 mW/m^2 (20 – 150

mW/m^2) according to the Intergovernmental Panel on Climate Change (IPCC) [2], of which contrail cirrus are estimated to account for ~80 % of this [3]. The lower bound of the contrail warming Confidence Interval (CI) is positive, showing that contrails have a net warming effect. In a review, Kärcher compared this figure with an estimate for the RF from aviation CO_2 (35 mW/m^2) [3] (Fig. 1). Allowing for the CIs, contrails are at best as relevant to global warming as CO_2 emissions. At worst, contrails could be a much larger contributor to global warming than CO_2. Further, the large CI indicates a large size of the contrail-related uncertainties. This resulted in contrails and cirrus cloud being given a *fair* and *very poor* Level of Scientific Understanding (LOSU) respectively by the IPCC in 1999 [4]. Industry and policymakers are unlikely to take steps to mitigate the climate impact of contrails if the uncertainty is high and the LOSU is *very poor*. It is hence a priority to reduce the uncertainty surrounding the net contrail radiative forcing (RF) and to improve the overall LOSU. Since the IPCC report, further research has taken place.

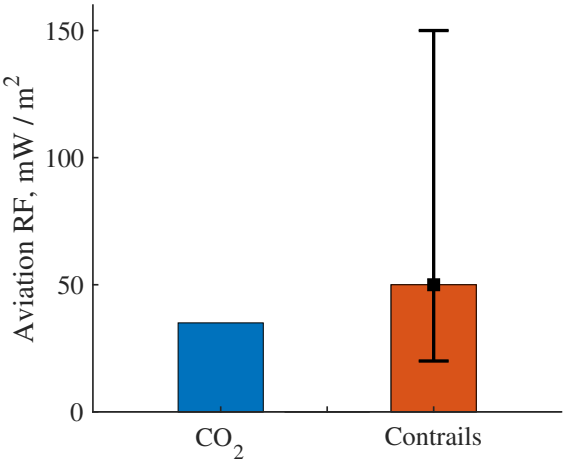

Fig. 1 Components of the aviation-induced radiative forcing. The CO_2 RF was obtained from [3]. The contrail RF was obtained from [2].

Computational models have collated legacy and new understanding of contrails, allowing the simulation of their lifecycle. Error bars given in IPCC charts are comprised of natural variability, model inadequacy, and scenario uncertainty [5]. Considering weather variability alone (a subset of natural variability), Monte Carlo runs conducted on a simple contrail model in [5] show large scatter of the results. It is concluded that uncertainty levels are unlikely to ever reach values considered acceptable [5]. This is aggravated if model inadequacy and scenario uncertainty are included. Despite the advancements in the field, the LOSU surrounding induced cirrus cloudiness was stated to be *very low* in 2005 [6]. The stance taken here is similar to that of [5]. In spite of the increased amount of data and understanding, estimating the net global warming effect remains difficult due to the high uncertainties of the weather data. Nevertheless, efforts to reduce contrail-induced warming should still be a strategic priority to tackle climate change.

The most effective way to eliminate contrail-induced RF is to prevent contrail formation. Contrail avoidance strategies, which require the use of contrail models alongside uncertainty management techniques, could be a way to achieve this. In a scenario in which contrail cirrus generating flights are to be redirected, airline dispatchers require knowing the probability of contrail cirrus being formed for each flight they operate. Dispatchers are estimated to work on a flight 1 to 2 hours prior to its departure [7, 8]. Contrail avoidance hence requires sufficient model speed to be a part of the workflow at dispatch (< ~2 hrs). Further, there is an unknown minimum contrail model accuracy since not all contrails are warming. Using models with low enough accuracy for avoidance could worsen the net warming effect.

Analyzing the suitability of existing contrail models for contrail avoidance is a necessary step in enabling contrail avoidance. Two prominent contrail models which are publicly available are APCEMM (developed at the Laboratory for Aviation and the Environment at MIT) [9], and CoCiP (developed at the German Aerospace Center) [10]. Computational models often have to compromise on either accuracy or speed. APCEMM focuses on accuracy by not assuming a contrail shape. CoCiP focuses on speed by assuming an elliptical contrail cross-section amongst other simplifying assumptions. On a machine with reasonable computing power, each CoCiP run takes ~2 s and each APCEMM run takes ~18.5 min. APCEMM is ~500 times slower than CoCiP. The differences in the behaviors of the two models are not yet understood.

This investigation aims to take the first steps towards the creation of a bespoke contrail prediction model for use in

contrail avoidance. First, the differences in the behaviors of APCEMM and CoCiP under certain and uncertain inputs will be documented and analyzed. Due to a lack of experimental results, this exercise will be solely comparative and will hence result in limited conclusions. In spite of this, this analysis will help determine the suitability of each model for contrail avoidance. Their performance will also provide with a baseline to compare the bespoke model with once it is developed. Further, this investigation also aims to provide an estimate for the minimum required accuracy for a contrail avoidance model. This minimum accuracy will be used as a threshold to determine whether the bespoke contrail avoidance tool is able to reduce the net warming from aviation.

Due to the high computational demand APCEMM poses, Non-Intrusive Polynomial Chaos has been chosen as the uncertainty management technique since it converges faster than traditional Monte Carlo methods. This allows for more stochastic experiments to be run with the same computing power. Furthermore, if a model was accurate enough to be used for contrail avoidance, NI-PCE would enable it to produce stochastic outputs faster than with traditional MC methods. This increased speed could make the model satisfy the time constraint to be included in the dispatch workflow. Beyond the comparison between the responses of each model to stochastic inputs, it is aimed to build a framework that expedites the production of stochastic results from any model.

The main goals of this investigation can now be summarized:

1) To compare the differences in behaviors between CoCiP and APCEMM under certain and uncertain inputs.
2) To estimate the minimum required accuracy for models to be used for contrail avoidance.

III. Background

A. Contrails, Contrail Cirrus, and Aircraft Plumes

Contrails are ice clouds initially formed by the condensation of the water in the exhaust of an aircraft when mixed with the cold ambient air [11]. They initially appear as straight cloud lines that are left behind by aircraft [3]. This section specifies the conditions for contrail formation, summarizes the stages in contrail evolution, and specifies how contrails contribute to global warming.

1. The Schmidt-Appleman Criterion for Contrail Formation

It is necessary for the Schmidt-Appleman criterion to be satisfied for the formation of a contrail [12]. This states that if the mixing line between exhaust conditions and ambient conditions intersects the liquid water saturation line, contrails will form (Fig. 2). It does not make any predictions regarding the lifespan or evolution of a contrail.

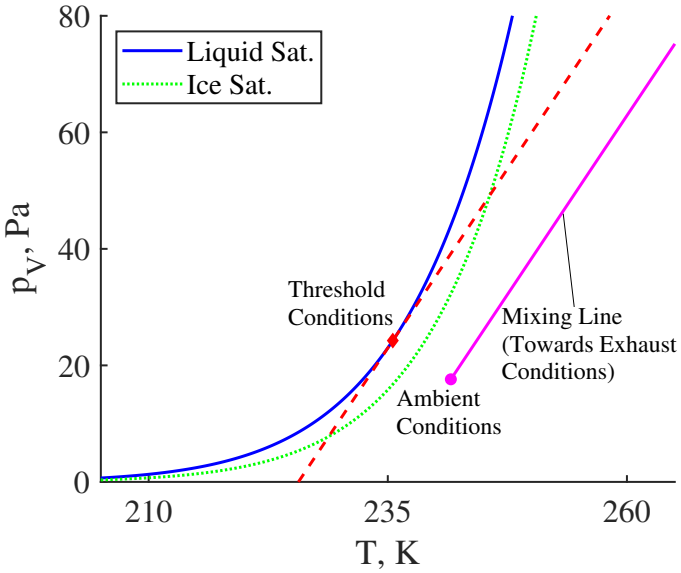

Fig. 2 Visualization of the Schmidt-Appleman criterion for contrail formation on a p_V-T chart. This figure takes direct inspiration from Fig. 5 in [13], and uses a fabricated scenario.

Assume a scenario in which the ambient conditions are not known *a priori* (but the exhaust conditions are). The threshold ambient conditions for contrail formation occur when the mixing line is tangent to the liquid water saturation line [12] (given by the solid blue line in Fig. 2). This is mathematically equivalent to the point where the gradient of the liquid water saturation line is equal to that of the mixing line m. The value of m is given by the following Eq. [10]:

$$m = \frac{c_p^{\text{air}}\ p_{atm}\ \text{EI}_{\text{H}_2\text{O}}}{M_{\text{ratio}}\ Q_{\text{fuel}}\ (1-\eta_{\text{ov}})} \tag{1}$$

Obtaining the tangent point temperature T_{LM} requires iterations and can hence be computationally expensive. An approximation for T_{LM} circumvents the need for iterations[10]:

$$T_{\text{LM}} \approx -46.46 + 9.43 \ln(m - 0.053) + 0.72 \left[\ln(m - 0.053)\right]^2 \tag{2}$$

With the tangent point, the threshold ambient conditions can now be obtained [10, 14]. The critical ambient relative humidity RH_{LC} is given by the following equation:

$$\text{RH}_{\text{LC}} = \frac{m \cdot (T_{atm} - T_{\text{LM}}) + p_{\text{sat}}^{\text{liq}}(T_{\text{LM}})}{p_{\text{sat}}^{\text{liq}}(T_{atm})} \tag{3}$$

Approximations for $p_{\text{sat}}^{\text{liq}}$ and $p_{\text{sat}}^{\text{ice}}$ are provided in [10].

2. The Evolution and Lifecycle of Contrails

If a contrail persists, the ambient relative humidity with respect to ice surpasses 100 % [13]. Persistent contrails evolve in the same manner as an aircraft plume. There are four main stages in the lifecycle of a persistent contrail: the Jet regime, the Vortex regime, the Dissipation regime, and the Diffusion regime [13].

The Jet regime (lasting until ∼10 s after generation [13]) is characterized by the entrainment of the jets from the engine into the aircraft vortex flow field. The aircraft vortices distort the jet cross-sections into ellipses [13] and the jet is cooled to ambient temperature [15]. The Vortex regime (from ∼10 s until ∼100 s after generation [13]) begins once the ice particle density is homogeneous in the axial and circumferential directions around the core of the vortex [13]. The vortices descend and bring down an oval-shaped cross-section of the air between them [13] that contains the exhaust plume [15]. During the vortex dissipation regime (from ∼100 s until ∼1000 s after generation [13]), stratification induces secondary vortices which interact with the unstable aircraft vortices, resulting in vortex breakup [13]. This leads to turbulence and hence a tenfold increase in the rate of entrainment between the exhaust plume and the ambient air [15]. The diffusion regime (from ∼1000 s after generation [13]) is dominated by atmospheric processes, rather than by aircraft-induced dynamics [15]. Examples of atmospheric processes that enable the wake spreading are turbulence, shear, and diffusion [13].

Contrail lifespan varies from seconds to hours, but it is only those contrails that reach the diffusion regime that can develop into wider cirrus-like cloud structures known as contrail cirrus. A contrail is considered to be long-lived if it remains for more than 10 minutes [3].

3. Contrails and Climate Change

Contrails are able to affect the climate by disturbing the radiation flux entering and leaving the planet (Fig. 3). First, contrails increase the albedo of the planet by reflecting part of the incoming Short-Wave (SW) radiation back to space [16], exclusively during the day [17]. Second, contrails reflect some outgoing Long-Wave (LW) radiation back towards the planet [16]. The Radiative Forcing (RF) of a contrail is then defined by:

$$\text{RF} = \text{RF}_{\text{LW}} - \text{RF}_{\text{SW}} \tag{4}$$

Where RF_{LW} is the component of the outgoing LW radiation reflected by the contrail, and RF_{SW} is the component of the incoming SW radiation reflected by the contrail (as in Fig. 3). The RF is defined to be positive when the contrail has a net warming effect, and negative when the contrail has a net cooling effect. Most studies conclude that the global net RF is positive [16], however some contrail segments can have a net cooling effect locally during the day [17].

Contrail cirrus account for approximately 80 % of the aforementioned RF [3]. Roughly ∼10 % of all contrails have a disproportionate effect on the net RF [5]. This implies that contrails that evolve into cirrus are rare compared to other warming contrails (∼80 % of all contrails [5]).

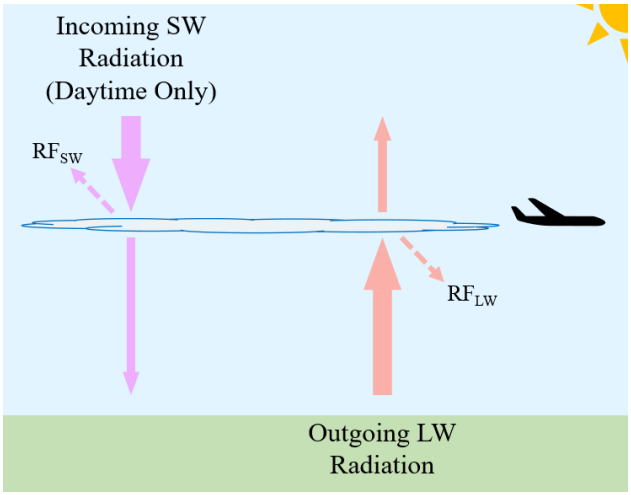

Fig. 3 Diagram showing radiative forcing components of contrails. This figure takes inspiration from Fig. 11 in [15].

B. Contrail Models

Four main types of contrail models have been developed: Single Plume (SP) model, Multi-layered Plume Models (MP), chemistry and microphysics-based models, and Large Eddy Simulations (LESs) [15].

The SP model assumes homogeneous (Gaussian) concentration distributions throughout the plume at each time step [15]. A two-dimensional diffusion equation that accounts for shear and distance from the plume center is then solved, resulting in a time-varying Gaussian function [15]. The homogeneous assumption made by the SP model is also its main drawback since it is only valid up to and including the vortex regime [15]. The MP model aims to capture the non-homogeneities after the vortex regime by dividing the plume cross-section into concentric rings. The SP model is used in each of these rings.

The most accurate family of contrail models employ LESs, but they are also the most computationally expensive [15]. Unlike Direct Numerical Simulation (DNS), which solves the Navier-Stokes equations numerically up to the Kolmogorov scale, LESs solve the Navier-Stokes equations only for large-scale eddies and use a model for the smaller scales [18]. LESs is faster than DNS, yet they are much more computationally expensive than the other types of contrail models [15]. This prevents LESs from being routinely run for the timescales required to model contrail cirrus, or for contrail avoidance.

1. CoCiP

The Contrail Cirrus Prediction Tool (CoCiP) is a SP model that was developed at the German Aerospace Center (DLR) [10]. It has seen extensive use in previous investigations. The version of CoCiP used in this investigation has been implemented by the Aviation Impact Accelerator (AIA) [19], based at the University of Cambridge. This version of CoCiP maintains the physical models as presented in [10].

To know whether a contrail forms, CoCiP uses the Schmidt-Appleman criterion (see Section III.A.1) [10]. CoCiP does not resolve the details of the plume during the jet and vortex regimes, but rather uses a parametric model to find estimates of the depth, width, and maximum and mean downward displacements of the plume at the start of the diffusion regime [10]. Each CoCiP run simulates a flight which is internally divided into waypoints. At each of these waypoints a contrail segment is generated, and its evolution is simulated. CoCiP produces contrail optical properties for each segment. The information of the geographical location, date, and time is then used to perform a radiative balance for each segment.

2. APCEMM

The Aircraft Plume Chemistry, Emissions, and Microphysics Model (APCEMM) is "a Lagrangian model that explicitly models the chemical and microphysical evolution of an aircraft plume" [9]. It was developed at the Laboratory for Aviation and the Environment at MIT. APCEMM is lower-level than MP models, but higher-level than LSE models.

Code for APCEMM has been publicly available at [20] since 2020.

Up to and inclusive of the vortex regimes, APCEMM considers the plume to be a well-mixed air mass, similar to the box model in [21]. At the diffusion regime, APCEMM uses concentric elliptical rings for the chemistry calculations. However, diffusion, advection, buoyancy, as well as other plume dynamics are simulated on a rectilinear grid [9]. The chemical constituents are then mapped from each elliptical ring to the grid, and transport is then computed [9]. Unlike CoCiP, APCEMM does not simulate a flight. Instead, it produces a single contrail segment and performs a high-fidelity simulation of its evolution. Further, APCEMM does not perform radiative balance on the segment. Nevertheless, it still produces the optical contrail properties.

C. Uncertainty Management With Non-Intrusive Polynomial Chaos

Contrail models are currently deterministic so propagating uncertainties requires the use of uncertainty management techniques. The technique chosen for this investigation is Non-Intrusive Polynomial Chaos (NI-PCE). This section describes the Wiener-Askey scheme and the point-collocation method from [22] for one-dimensional NI-PCE. Details for multidimensional NI-PCE can be found in [22] and in [23].

Polynomial Chaos Expansion (PCE) is a technique which enables the spectral decomposition of random variables into orthogonal probability spaces. PCEs express random variables as a sum of the products of deterministic terms and non-deterministic terms (Eq. 6). These decomposed distributions of the random variables can then be propagated throughout the model to obtain model outputs with corresponding distributions. PCE uses the Wiener-Askey scheme.

Consider a random process with bounded moments $X(\theta)$, which is a function of the random event θ. This process can be split into deterministic and stochastic components:

$$X(\theta) = \sum_{j=0}^{\infty} x_j \Phi_j(\xi) \tag{5}$$

Where x_j are the deterministic coefficients, and $\Phi_j(\xi)$ are orthogonal polynomials evaluated at the output of a random process ξ (the germ).

Note that ξ is a function of the random event θ, making ξ and $X(\theta)$ dependent random variables. In this decomposition, $X(\theta)$ is known or can be estimated, and both ξ and $\Phi(\xi)$ are choices to be made [24]. The type of orthogonal polynomial used is necessarily determined by the choice of germ (see Table 4.1 in [24]). Implementation requires the truncation of Eq. 5 to a maximum order P:

$$X(\theta) = \sum_{j=0}^{P} x_j \Phi_j(\xi) \tag{6}$$

The aim is now to find the coefficients x_j. This can be done by projecting $X(\theta)$ along the j-th orthogonal direction in the Hilbert space spanned by the orthogonal polynomials Φ. For this, an inner product in this space is defined for two functions $f(\xi)$ and $g(\xi)$ [24]:

$$\langle f(\xi) g(\xi) \rangle = \int_{-\infty}^{\infty} f(\xi) g(\xi) W(\xi) d\xi \tag{7}$$

The function $W(\xi)$ is the probability density function (PDF) of the germ ξ. Note that the ξ and $\Phi(\xi)$ pairs have been chosen such that $\langle \Phi_i \Phi_j \rangle = \langle \Phi_i^2 \rangle \delta_{ij}$, where δ_{ij} is the Kronecker delta [24]. This inner product can be applied to both sides of Eq. 6 to obtain the coefficient x_i. Dropping the θ and ξ, and assuming the integer $i \in [0, P]$:

$$\langle X \Phi_i \rangle = \sum_{j=0}^{P} x_j \langle \Phi_i \Phi_j \rangle = x_i \langle \Phi_i^2 \rangle \tag{8}$$

Rearranging, the Spectral Galerkin Projection is obtained:

$$x_i = \frac{\langle X \Phi_i \rangle}{\langle \Phi_i^2 \rangle} \tag{9}$$

The term $\langle X(\theta) \Phi_i(\xi) \rangle$ in the numerator of Eq. 9 cannot be evaluated directly because the relationship between $X(\theta)$ and ξ is not known. These variables can be related to each other through the use of a third random variable $u \sim U[0,\ 1]$

[24]. It is shown in [24] that the variables X, ξ, and u can be related by the use of the cumulative distribution function (CDF) of X and ξ ($F(X)$ and $G(\xi)$ respectively).

$$u = F(X) = G(\xi) \tag{10}$$

Defining $h(u) = F^{-1}(u) = X$, and $l(u) = G^{-1}(u) = \xi$, the term $\langle X(\theta)\Phi_i(\xi)\rangle$ can be evaluated by changing the integration variable from ξ to u [24]. This is known as a double Rosenblatt transformation, and gives the following integral:

$$\langle X(\theta)\Phi_i(\xi)\rangle = \int_0^1 h(u)\Phi_i(l(u))du \tag{11}$$

The coefficients in Eq. 6 can now be evaluated using Eqs. 9 and 11. These equations allow for the performance of NI-PCE.

Consider a system with an input random parameter $K(\xi)$, and output a variable of interest $Y(\xi)$. The spectral expansion of $Y(\xi)$ will have $P+1$ deterministic coefficients y_j to be found (Eq. 6), and will use the same orthogonal polynomials $\Phi_j(\xi)$ as $K(\xi)$. Now the germ ξ is sampled at least $P+1$ times, resulting in a list of germ samples ξ_i^* ($i = 0, 1, 2, ...N$, $N \geq P+1$). These samples can be used to find corresponding samples of the parameter K_i^*, since K depends on ξ. A set of samples of the output Y_i^* can be found using the deterministic model with the corresponding K_i^* as the parameter. These data can be placed in a matrix equation of the form $\mathbf{Ax} = \mathbf{b}$, for which $\mathbf{x}$ needs to be solved.

$$\begin{bmatrix} \Phi_0(\xi_0^*) & \Phi_1(\xi_0^*) & \dots & \Phi_P(\xi_0^*) \\ \Phi_0(\xi_1^*) & \Phi_1(\xi_1^*) & \dots & \Phi_P(\xi_1^*) \\ \vdots & \vdots & \ddots & \vdots \\ \Phi_0(\xi_N^*) & \Phi_1(\xi_N^*) & \dots & \Phi_P(\xi_N^*) \end{bmatrix} \begin{bmatrix} y_0 \\ y_1 \\ \vdots \\ y_P \end{bmatrix} = \begin{bmatrix} Y_0^* \\ Y_1^* \\ \vdots \\ Y_N^* \end{bmatrix} \tag{12}$$

Where $\mathbf{A}$ is the matrix containing the basis orthogonal polynomials evaluated at each sampled germ ξ_i^*, $\mathbf{x}$ is the vector containing the unknown coefficients of the spectral expansion of Y, and $\mathbf{b}$ is the vector containing the sample outputs of the deterministic model evaluated at the corresponding ξ_i^*.

IV. Methods

A. Interfacing With CoCiP and APCEMM

The comparison between two models requires the classification and comparison of the inputs and outputs. This section aims to specify which of the inputs are to be treated as independent variables, which inputs are to be chosen as constants between the two models, and which outputs are to be treated as dependent variables.

Table 1 provides a high-level comparison between the types of inputs available in APCEMM and CoCiP. As discussed in Section III.A.1, contrail formation requires the ambient relative humidity surpassing a critical value. An alternative formulation which specifies a critical temperature beneath which contrails will form is also used [12]. Since both the relative humidity and the temperature determine contrail formation, they have been chosen as the independent variables in this study. The relative humidity and temperature values are enforced within a moist layer, spanning 1000 m vertically and centered at the cruise altitude. Table 1 shows that the relative humidity in CoCiP is relative to ice saturation, whereas the relative humidity in APCEMM is relative to vapor saturation. Converting between these requires the use of the following equation:

$$\mathrm{RH}_{\mathrm{ice}} = \mathrm{RH}_{\mathrm{liq}} \frac{p_{\mathrm{sat}}^{\mathrm{liq}}(T)}{p_{\mathrm{sat}}^{\mathrm{ice}}(T)} \tag{13}$$

Where RH is the relative humidity.

The remaining variables in Table 1 have been assigned a constant value throughout the experiments conducted. These values are available in Table 2. Parameters omitted from Table 2 have been set to the default values in their respective models. The aircraft type parameters referring to the core exit temperature and the exit bypass area have also been left as the default in APCEMM since reliable values for these were not obtained.

The main outputs of interest of both CoCiP and APCEMM have been provided in Table 3. APCEMM does not perform a radiation balance on the contrail segment so comparing RF between APCEMM and CoCiP is not possible (see Sections III.B.1 and III.B.2). Though both CoCiP and APCEMM output optical depth values, APCEMM provides the

optical depth of each grid cell. Equating this and the average vertical optical depth from CoCiP is non-trivial, requiring assumptions of the contrail shape. The optical depth is therefore not suitable for comparison. The remaining parameter that is related to the optical properties of the contrail is the number of ice crystals per unit length, which can be directly compared between CoCiP and APCEMM. This was chosen as the first dependent variable. The second dependent variable was chosen to be the ice mass of the contrail per unit length (α) because it is an indicator of contrail life. The comparison of contrail ice mass is not direct because in CoCiP it is given per kg of air (I), whereas in APCEMM it is given per unit contrail length:

$$\alpha = \rho_{atm} S I \tag{14}$$

Where S is the contrail cross-sectional area.

Table 1 Comparison of the inputs in CoCiP and APCEMM. Some entries in this table refer to a family of inputs. The italicized entries indicate the independent variables chosen for this investigation.

Input Quantity	Available in CoCiP?	Available in APCEMM?	Direct Translation?	Notes
Relative Humidity	*Y*	*Y*	*N*	*CoCiP RH is relative to ice.*
Ambient Temperature	*Y*	*Y*	*Y*	
Lat. and Lon.	Y	Y	Y	
Altitude	Y	Y	N	APCEMM uses pressure.
Cruise Speed	Y	Y	Y	
Aircraft Params.	Y	Y	N	APCEMM has more params.
Aircraft Performance	Y	Y	N	CoCiP uses overall efficiency only.
Emissions Params.	Y	Y	N	APCEMM has more params.
Contrail Params.	Y	Y	N	APCEMM has more params.

Table 2 Values of the shared parameters chosen for CoCiP and APCEMM. Parameters omitted here have remained at their default value of their respective model.

Parameter	Value	Units	Notes
Latitude	53.55	°	
Longitude	-1.58	°	
Altitude	36000	ft	Equivalent to 227 hPa using the standard atmosphere.
Cruise Speed	250.9	m/s	True airspeed.
Aircraft Type	A350	—	
Aircraft Mass	224658	kg	Measured at the generation of the contrail segment.
Horizontal Diffusion Coefficient	15.00	m^2/s	
Vertical Diffusion Coefficient	0.15	m^2/s	
Brunt–Väisälä Frequency	0.01	Hz	

Table 3 Comparison of the outputs in CoCiP and APCEMM. The italicized entries indicate the dependent variables chosen for this investigation.

Output Quantity	Available in CoCiP?	Available in APCEMM?	Direct Translation?	Notes
Radiative Forcing	Y	N	N	
Optical Depth	Y	Y	N	Provided as a grid in APCEMM.
Extinction Coefficient	Y	Y	N	Provided as a grid in APCEMM.
Number of Ice Particles	*Y*	*Y*	*Y*	
Ice Mass	*Y*	*Y*	*N*	*CoCiP normalizes per kg of air.*
Contrail Width	Y	Y	Y	
Contrail Depth	Y	Y	Y	
Contrail Area	Y	N	N	

B. Design of Experiment

With a choice of the dependent and independent variables, the experimental plan is now specified:

- **Experiment 1:** A deterministic parameter sweep of the independent variables.
- **Experiment 2:** A multivariate stochastic run of the models using NI-PCE.

First, the response of the models to deterministic inputs will be measured. A sweep of the independent variables will be used for this. The dependent variables will be graphed at t = 50 min to capture the persistent contrails only (t > 10 min). The results will indicate the most sensitive regions of the model, which will be used to build the distributions for the NI-PCE run. The details of the parameter sweep are given in Table 4. The parameters are varied individually. The default value of a parameter is used when the other parameter is being varied:

- $\mathrm{RH}_{\mathrm{liq,\ default}}$ = 100 %
- T_{default} = 217 K

The stochastic run has two objectives. The first objective is to determine the sensitivity of the models to temperature and relative humidity. The second objective is to compare the time evolution of the persistent contrails in each model. To do this, multivariate NI-PCE is performed taking one distribution for each of the independent variables. Since neither of the dependent variables can be negative, a distribution with a hard lower bound is preferred for faster NI-PCE convergence. Further, it was chosen to avoid the use of skewed distributions to ensure that the sensitivity of the model is represented accurately. The simplest distribution satisfying both of these conditions is the uniform distribution. Details of the distributions of each independent variable are now given:

- $\mathrm{RH}_{\mathrm{liq}}$ ~U(100, 110) %
- T ~U(215, 225) K

Further, the sampling of the distributions has been seeded to ensure the reproducibility of the results. Contrail segments are only simulated for a maximum of six hours in APCEMM.

Table 4 Values of taken by the independent variables in the deterministic parameter sweep.

Parameter	Units	Start Value	End Value	Step size
$\mathrm{RH}_{\mathrm{liq}}$	%	0	140	5
T	K	207	237	1

C. Software Details

The experiments performed in this investigation have been scripted in `Python`. The package `chaospy` (available in [25]) [23, 26] has been used to perform NI-PCE following the documentation in [27]. The version of APCEMM used in this investigation is publicly available at [20].

V. Results and Discussion

A. Parameter Sweep Results

The effects of the parameter sweeps on the ice particle numbers for both CoCiP and APCEMM are shown in Figs. 4 and 5. As expected, a critical temperature and a critical relative humidity is observed in both models. The critical RH_{liq} is 60 % for both models, which corresponds to a RH_{ice} value of 104 % at T = 217 K. The previous point (RH_{liq} = 55 %) corresponds to a RH_{ice} value of 96 %. Figures 4 and 5 only sample from persistent contrails (samples taken at t = 50 min). Therefore, these results are consistent with the fact that $RH_{ice} > 100$ % for contrails to persist [13]. Further, the critical ambient temperature is 230 K for APCEMM and 229 K for CoCiP. The discrepancy of these figures is small and hence negligible.

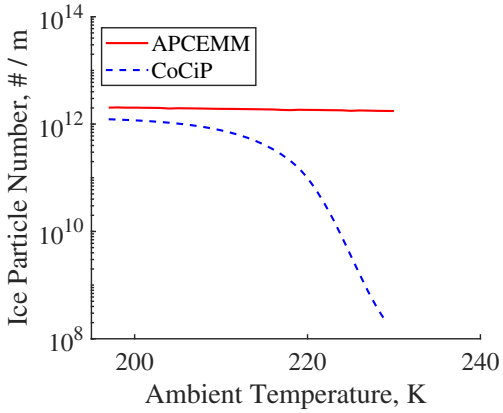

Fig. 4 Variation of ice particle number with ambient temperature at t = 50 min. RH_{liq} = 100 %.

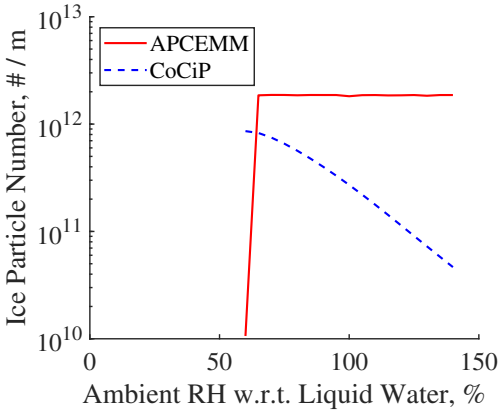

Fig. 5 Variation of ice particle number with relative humidity at t = 50 min. T = 217 K.

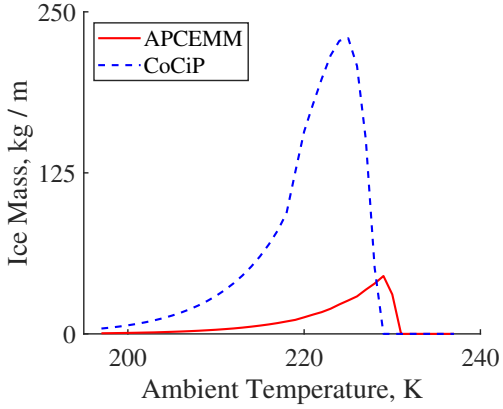

Fig. 6 Variation of contrail mass with ambient temperature at t = 50 min. RH_{liq} = 100 %.

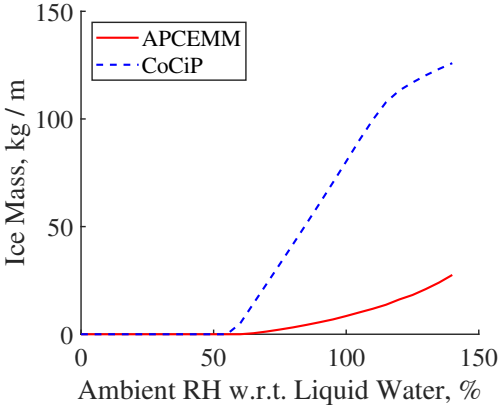

Fig. 7 Variation of contrail mass with relative humidity at t = 50 min. T = 217 K.

In Fig. 4, as the critical temperature is approached, the number of ice particles in APCEMM remains roughly constant, but the number of ice particles in CoCiP decreases at a progressively higher rate. This loss rate increases until reaching a steady exponential decay with decay constant of 0.72, given by the straight section beginning at T = 222 K. A similar phenomenon occurs in Fig. 5, where the number of ice particles produced by CoCiP experiences an exponential decay with increasing RH_{liq} at $RH_{liq} > 80$ %. The decay constant for the CoCiP curve in Fig. 5 is 0.04.

In Fig. 5 the number of ice particles produced by APCEMM is approximately constant (except for when RH_{liq} = 60 %). Although the orders of magnitude of the sweep responses are originally similar, APCEMM and CoCiP display significantly different behaviors. This discrepancy cannot be yet attributed to anything.

Figures 6 and 7 show the variation of contrail ice mass to the parameter sweep for CoCiP and APCEMM. The critical RH_{liq} is observed to be 60 %, consistent with Fig. 5. The discrepancy in the critical temperature has increased by 1 K (228 K for CoCiP and 230 K for APCEMM). This is still negligible. Figure 6 shows that the contrail ice mass has a peak for both CoCiP and APCEMM before reaching the critical temperature. Like with the critical temperature, the CoCiP peak lags behind the APCEMM peak. The CoCiP peak is also 5 times larger than the APCEMM peak. In spite of the discrepancy in magnitude, the behaviors towards a change in temperature exposed by both models agree. Figure 7 shows that the ice mass in both CoCiP and APCEMM increases after the critical RH_{liq} is reached. The response generated by CoCiP initially increases linearly with a gradient of 1.8 kg/%. The APCEMM response is non-linear, and has an average gradient lower than that of CoCiP. Disregarding the difference in the magnitudes of the response, there is agreement in the high-level behavior of CoCiP and APCEMM.

The T runs have shown that the most sensitive parts of the responses occur in the range [215 — 225 K] for persistent contrails. Further, the most sensitive parts of the responses to RH_{liq} occur when $RH_{liq} > 60$ %. The uniform distributions from Section IV.B have bounds that ensure lying in a sensitive portion of each model.

B. NI-PCE Results

The effects of uncertainty on the time evolution of contrail properties are shown in Figs. 8, 9, 10, and 11.

Consider first the evolution of the APCEMM contrail properties (Figs. 8, 9). Figure 8 shows that the number of ice particles decays slowly with time, remaining at the same order of magnitude. The uncertainty for the number of ice particles is very low for APCEMM, but grows in time. This growth of the uncertainty with time is expected as the contrail does not appear to be dying, If the contrail were dying, convergence of the uncertainty towards the mean would be expected. Figure 9 shows that the contrail ice mass is generally growing with time, and continues to do so at the end of the simulation. This indicates that the contrail continuing to expand throughout the simulation. The uncertainty appears to reach a constant value after t = 150 min. The standard deviation displayed in this region is approximately 19 kg. This is a significant uncertainty that shows that APCEMM is very sensitive to weather data.

Consider now the evolution of the CoCiP contrail properties (Figs. 10, 11). Figure 10 shows that the ice particle number experiences an exponential decay followed by a jump towards zero. The decay constant of the exponential section is 0.09. In Fig. 10 the uncertainty appears to increase as the contrail dissipates. This increase in uncertainty is an artifact of the logarithmic scaling since zero is reached by the lower bound first. This causes the vertical drop-off observed. In the absolute sense, the uncertainty converges as the contrail dissipates. Nevertheless, the uncertainties do grow before this effect becomes relevant. Figure 11 shows that the contrail ice mass peaks at t = 46 min and then decays. The fact that the ice number decays exponentially whilst the ice mass increases when $t < 46$ min indicates that the ice crystal size is growing in this region. The magnitude of the uncertainties also peaks at t = 46 min and then decays. Here, the standard deviation reaches a value of 72 kg. Overall, CoCiP is very sensitive to the input weather data.

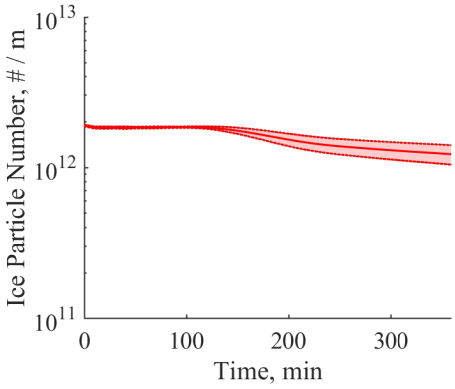

Fig. 8 Uncertain time evolution of the contrail section ice particle number in APCEMM. The solid line indicates the mean, and the shaded area is bounded by $\pm\sigma$ from the mean.

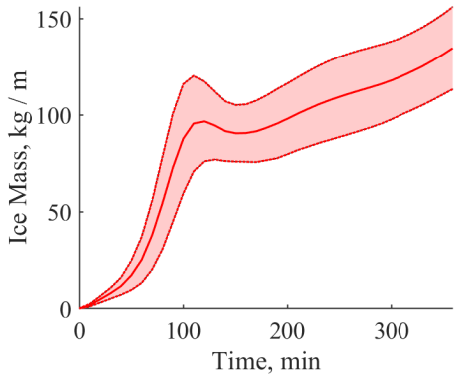

Fig. 9 Uncertain time evolution of the contrail section ice mass in APCEMM. The solid line indicates the mean, and the shaded area is bounded by $\pm\sigma$ from the mean.

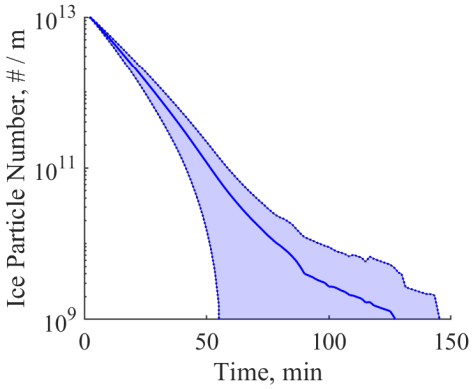

Fig. 10 Uncertain time evolution of the contrail section ice particle number in CoCiP. The solid line indicates the mean, and the shaded area is bounded by $\pm\sigma$ from the mean.

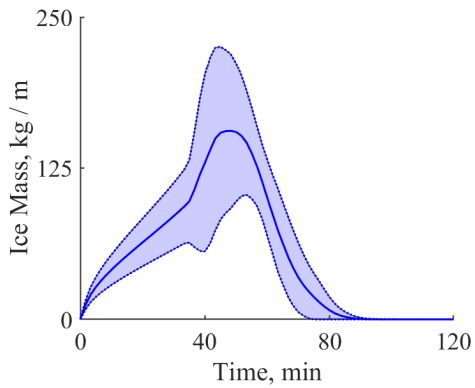

Fig. 11 Uncertain time evolution of the contrail section ice mass in CoCiP. The solid line indicates the mean, and the shaded area is bounded by $\pm\sigma$ from the mean.

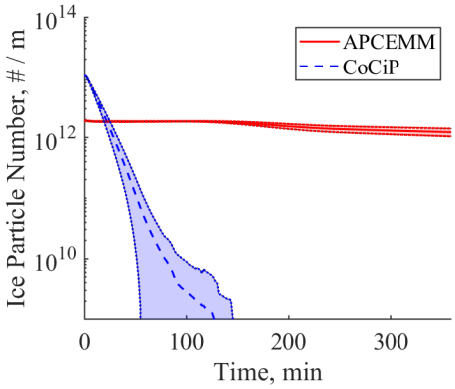

Fig. 12 Uncertain time evolution of the contrail section ice particle number in APCEMM (red line) and CoCiP (blue dashed line). The solid lines indicate the corresponding mean, and the shaded area is bounded by $\pm\sigma$ from the mean.

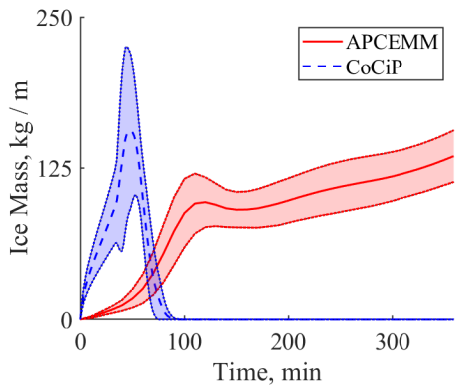

Fig. 13 Uncertain time evolution of the contrail section ice mass in APCEMM (red line) and CoCiP (blue dashed line). The solid lines indicate the corresponding mean, and the shaded area is bounded by $\pm\sigma$ from the mean.

C. Interim Conclusion

The analysis of the parameter sweep results suggests that CoCiP and APCEMM could be made to agree if the remaining parameters are adjusted and a correction is applied. It remains unknown which model behavior is closer to reality. A comparison between the CoCiP and APCEMM stochastic runs is available in Figs. 12 and 13. The contrail segment simulated in CoCiP decays faster and has the largest uncertainties. APCEMM appears to be less sensitive to the weather inputs, with its uncertainty being approximately constant for its evolution. The model time responses are overall significantly different. In addition to the fact that the sensitivity to input uncertainties is large, there is a clear need for increasing the amount of appropriate validation data for such an experiment. Nevertheless, to determine the suitability of each model for contrail avoidance it is required to know what their minimum accuracy should be. With scarce knowledge of real contrail behavior, the minimum required accuracy can be estimated by considering a simplified model scenario in which the model has a binary choice to be made (this choice consists of deciding whether there will be persistent contrail cirrus or not). This analysis is performed in Section VI.

VI. Estimating the Minimum Required Accuracy for Contrail Avoidance

Diverting aircraft from their optimal great-circle path results in a fuel consumption penalty. Current commercial flights do not necessarily follow the optimal great-circle paths, meaning that diversions could result in either a fuel burn benefit or penalty, without accounting for winds. The analysis performed in this section assumes that diverting a flight always results in a fuel burn penalty.

For contrail avoidance the use of models is required to predict what contrails can develop into contrail cirrus. A good avoidance strategy ensures that fuel burn penalty incurred is outweighed by the savings in contrail RF. A poor avoidance strategy could worsen the existing climate impact. Therefore, a minimum acceptable accuracy is required of the contrail models to be used for prediction. To determine this critical accuracy, a probability tree diagram (Fig. 14) has been used to create a table containing the elements of a confusion matrix (Table 5). No numerical values for the True Positive Rate (TPR), False Negative Rate (FNR), False Positive Rate (FPR), and True Negative Rate (TNR) are included in these figures. Note that this representation of the scenarios is binary, and is therefore a simplification of reality.

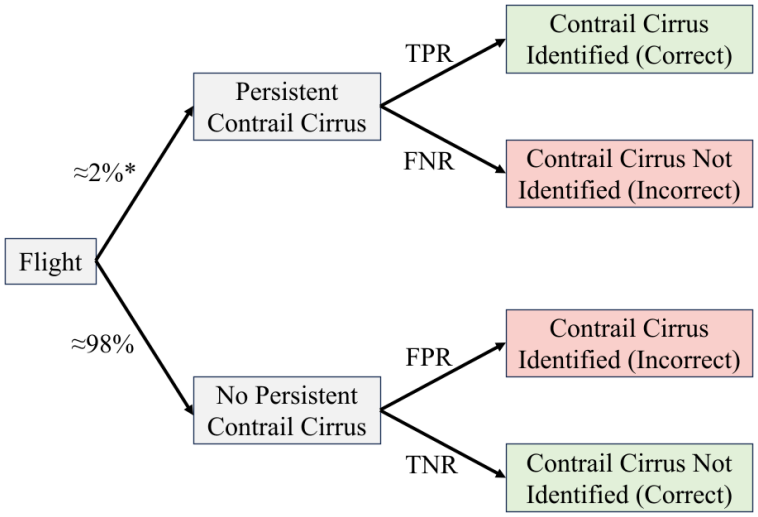

Fig. 14 Probability tree for the model identification of a contrail. The two percent of flights resulting in contrail cirrus is an extrapolation of the following result from [28]: 2.2 % of flights result in 80 % of the contrail energy forcing.

Table 5 Table showing the radiative effects of the different scenarios from Fig. 14 relative to current aircraft RF emissions. Preventing a contrail cirrus cloud from forming has a benefit of 28 Wm^{-2}, which is 70 % (see [29]) of the net RF due to contrail cirrus [3]. Performing an avoiding action has a penalty of 0.5 $Wm^{-}2$ (see [29]), which is ∼1.5 % of the net RF due to carbon [3]. The values in this table are illustrative only.

Scenario	Rates	ΔRF_{AIC} (Wm^{-2})	ΔRF_{CO_2} (Wm^{-2})	Proportion of Flights (%)
True Positive	TPR	-28.0	0.5	2 %
False Negative	FNR	0.0	0.0	
False Positive	FPR	0.0	0.5	98 %
True Negative	TNR	0.0	0.0	

Assuming that the TPR and TNR are equal, they are also equal to the accuracy metric Λ. It follows that FNR = FPR = 1 - Λ. The minimum model accuracy is defined as that which result in a negative expected RF:

$$\mathbb{E}(\mathrm{RF}) = 0.02 \cdot \Lambda \cdot (\Delta\mathrm{RF}_{\mathrm{AIC}} + \Delta\mathrm{RF}_{\mathrm{CO_2}}) + 0.98 \cdot (1 - \Lambda) \cdot \Delta\mathrm{RF}_{\mathrm{CO_2}} \tag{15}$$

$$\Lambda > \frac{0.98 \cdot \Delta\mathrm{RF}_{\mathrm{CO_2}}}{0.96 \cdot \Delta\mathrm{RF}_{\mathrm{CO_2}} - 0.02 \cdot \Delta\mathrm{RF}_{\mathrm{AIC}}} \tag{16}$$

With Eq. 15 and the changes in RF from Table 5, a lower bound for the required model accuracy is calculated to be 47 %. This is a lower bound for several reasons. First, in general the TPR does not equal the TNR. There could also be cases in which diverting when there is no contrail cirrus could lead to the formation of additional contrail cirrus. Further, the RF from normal contrails has also been neglected. To produce a more robust estimate, contours of Λ have been produced (Fig. 15). These contours show that if at least 50 % of the RF associated to contrail cirrus can be avoided, Λ is primarily sensitive to the fuel burn RF penalty. The point computed above (the *nominal point*) lies within this region. The sensitivity of Λ towards the fuel burn penalty is investigated by graphing Λ as a function of $\Delta\mathrm{RF}_{\mathrm{CO_2}}$ through the *nominal point* (Fig. 16). Although [29] claims that a fuel penalty of 1.5 % results in a reduction of 70 % of the contrail length (which represents the *nominal point*), in practice fuel burn penalties are likely to be higher. Allowing for double the fuel burn penalty claimed in [29] (3 %), a minimum accuracy of ~65 % is obtained. The choice of doubling the allowed fuel burn penalty is arbitrary. In spite of this and of above simplifying assumptions, this exercise has shown that contrail models do not need to be very accurate (>~65 %) to reduce the climate impact from contrails.

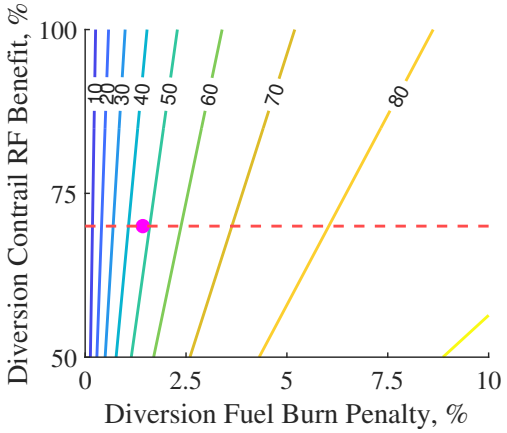

Fig. 15 Contours of minimum accuracy Λ for different values of $\Delta\mathrm{RF}_{\mathrm{CO_2}}$ on the x-axis and $\Delta\mathrm{RF}_{\mathrm{AIC}}$ on the y-axis. These have been expressed as percentages of the respective net RF values. The magenta dot shows the nominal value. The dashed red line shows the cross-section graphed in Fig. 16.

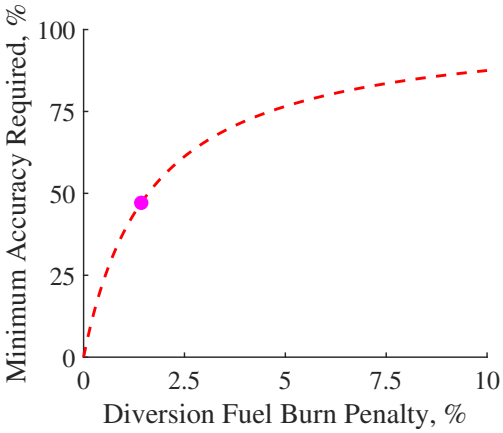

Fig. 16 Minimum required accuracy Λ vs fuel burn penalty $\Delta\mathrm{RF}_{\mathrm{CO_2}}$. The value of $\Delta\mathrm{RF}_{\mathrm{CO_2}}$ has been expressed as a percentage of its net RF value. The magenta dot shows the nominal value used in the above analysis. This graph is the cross-section of Fig. 15 along the dashed red line.

VII. Conclusion

This investigation had two objectives to take the first steps towards creating a bespoke model for contrail avoidance. The first objective was to perform a high-level comparison between CoCiP and APCEMM. This was necessary in order to provide with a baseline to compare the future model to, and to determine the level of agreement between existing models. The second objective was to provide an estimate for the minimum accuracy required for models to be used for contrail avoidance.

First, the comparison between CoCiP and APCEMM revealed that the response to changing temperature and relative humidity is similar from a high level. However, the stochastic experimental run showed that the time response of the models do not agree, and that both models are sensitive to input uncertainties. CoCiP appears to be significantly more sensitive to input uncertainties than APCEMM. The disagreement of the time response and the high sensitivity to the weather data only allow for the conclusion that an increased amount of appropriate data is needed to validate the

evolution of contrails in each model. This will allow the models to be adjusted to reflect the real contrail behavior. Currently, adjusting the models to agree amongst themselves is likely to be possible if further parameters were adjusted and a correction was applied to the results. However, doing this would assume that one model is closer to reality than the other. This could prevent the discovery of a physical mechanism that could explain some discrepancy between the models and reality.

Second, by assuming that contrail prediction models have a binary output, the minimum accuracy required for a contrail prediction model has been estimated to be ∼65 %. This has been calculated on the basis that all correct and incorrect decisions to avoid a contrail-forming region need to have at least a neutral climate impact. A minimum accuracy of ∼65 % is low, hence implying that simple models could be suitable for contrail prediction and avoidance.

In conclusion, the first steps towards creating a bespoke contrail model for avoidance have been taken. With the discovery that the available contrail models do not generally agree on contrail evolution, the primary conclusion of this investigation is that appropriate validation data will be needed to compare between existing and future models. Future work in the comparison of exiting models should also be done regarding the sensitivity of the models to changes in their parameters under fixed meteorological conditions.

Acknowledgments

C. Akhtar Martínez and J. P. Jarrett thank Dr. James Taylor and Dr. Jessie R. Smith for reviewing the work presented. The authors also thank Dr. Sebastian Eastham for the technical help provided. This work was supported by the UK Engineering and Physical Sciences Research Council [grant number EP/W524633/1]. For the purpose of open access, the authors have applied a Creative Commons Attribution (CC BY) license to any Author Accepted Manuscript version arising.

References

[1] Ritchie, H., "Climate change and flying: what share of global CO2 emissions come from aviation?" Our World in Data, Oct. 2020. URL https://ourworldindata.org/co2-emissions-from-aviation, accessed on May 14, 2023.

[2] Boucher, O., Randall, D., Artaxo, P., Bretherton, C., Feingold, G., Forster, P., Kerminen, V.-M., Kondo, Y., Liao, H., Lohmann, U., Rasch, P., Satheesh, S., Sherwood, S., Stevens, B., and Zhang, X., "Clouds and Aerosols," *Climate Change 2013: The Physical Science Basis. Contribution of Working Group I to the Fifth Assessment Report of the Intergovernmental Panel on Climate Change*, 2013, Cambridge University Press, Cambridge, United Kingdom and New York, NY, USA. URL https://www.ipcc.ch/site/assets/uploads/2018/02/WG1AR5_Chapter07_FINAL-1.pdf, accessed on May 14, 2023.

[3] Kärcher, B., "Formation and radiative forcing of contrail cirrus," *Nature Communications*, Vol. 9, 2018, Nature Publishing Group. https://doi.org/10.1038/s41467-018-04068-0.

[4] Penner, J. E., Lister, D., Griggs, D. J., Dokken, D. J., and McFarland, M., *Aviation and the global atmosphere: a special report of the Intergovernmental Panel on Climate Change*, Cambridge University Press, 1999. URL https://books.google.ie/books?id=JgphajrWfOsC&printsec=frontcover#v=onepage&q&f=false, accessed on July 25, 2023.

[5] Wilhelm, L., Gierens, K., and Rohs, S., "Weather Variability Induced Uncertainty of Contrail Radiative Forcing," *Aerospace*, Vol. 8, No. 11, 2021, p. 332. https://doi.org/10.3390/aerospace8110332.

[6] Lee, D. S., Fahey, D. W., Forster, P. M., Newton, P. J., Wit, R. C., Lim, L. L., Owen, B., and Sausen, R., "Aviation and global climate change in the 21st century," *Atmospheric Environment*, Vol. 43, No. 22, 2009, pp. 3520–3537. https://doi.org/10.1016/j.atmosenv.2009.04.024.

[7] Herstam, J., "It Takes A Village: What's Involved In Making On-Time Departures Possible," Simple Flying, Nov. 2022. URL https://simpleflying.com/on-time-departures-roles-involved/, accessed on May 23, 2023.

[8] Sowsun, M., "How long does flight planning take / when is it done / how is it done?" Stack Exchange, June 2016. URL https://aviation.stackexchange.com/a/27989, accessed on May 23, 2023.

[9] Fritz, T. M., Eastham, S. D., Speth, R. L., and Barrett, S. R. H., "The role of plume-scale processes in long-term impacts of aircraft emissions," *Atmospheric Chemistry and Physics*, Vol. 20, No. 9, 2020, pp. 5697–5727. https://doi.org/10.5194/acp-20-5697-2020.

[10] Schumann, U., "A contrail cirrus prediction model," *Geoscientific Model Development*, Vol. 5, No. 3, 2012, pp. 543–580. https://doi.org/10.5194/gmd-5-543-2012.

[11] Sanz-Morère, I., Eastham, S. D., Speth, R. L., and Barrett, S. R. H., "Reducing Uncertainty in Contrail Radiative Forcing Resulting from Uncertainty in Ice Crystal Properties," *Environ Sci Technol Lett*, Vol. 7, No. 6, 2020, pp. 371–375. https://doi.org/10.1021/acs.estlett.0c00150.

[12] Schumann, U., "On Conditions for Contrail Formation from Aircraft Exhausts," *Meteorologische Zeitschrift*, Vol. 5, 1996, pp. 4–23. URL https://elib.dlr.de/32128/, accessed on May 17, 2023.

[13] Paoli, R., and Shariff, K., "Contrail Modeling and Simulation," *Annual Review of Fluid Mechanics*, Vol. 48, No. 1, 2016, pp. 393–427. https://doi.org/10.1146/annurev-fluid-010814-013619.

[14] Ponater, M., Marquart, S., and Sausen, R., "Contrails in a comprehensive global climate model: Parameterization and radiative forcing results," *Journal of Geophysical Research: Atmospheres*, Vol. 107, No. D13, 2002, pp. ACL 2–1–ACL 2–15. https://doi.org/10.1029/2001JD000429.

[15] Tait, K. N., Khan, M. A. H., Bullock, S., Lowenberg, M. H., and Shallcross, D. E., "Aircraft Emissions, Their Plume-Scale Effects, and the Spatio-Temporal Sensitivity of the Atmospheric Response: A Review," *Aerospace*, Vol. 9, No. 7, 2022. https://doi.org/10.3390/aerospace9070355.

[16] Schumann, U., Bugliaro, L., Dörnbrack, A., Baumann, R., and Voigt, C., "Aviation Contrail Cirrus and Radiative Forcing Over Europe During 6 Months of COVID-19," *Geophysical Research Letters*, Vol. 48, 2021, Blackwell Publishing Ltd. https://doi.org/10.1029/2021GL092771.

[17] Meerkötter, R., Schumann, U., Doelling, D. R., Minnis, P., Nakajima, T., and Tsushima, Y., "Radiative forcing by contrails," *Annales Geophysicae*, Vol. 17, No. 8, 1999, pp. 1080–1094. https://doi.org/10.1007/s00585-999-1080-7.

[18] Zhiyin, Y., "Large-eddy simulation: Past, present and the future," *Chinese Journal of Aeronautics*, Vol. 28, No. 1, 2015, pp. 11–24. https://doi.org/10.1016/j.cja.2014.12.007.

[19] "Aviation Impact Accelerator," Aviation Impact Accelerator, University of Cambridge, 2023. URL https://www.aiazero.org/, accessed on August 10, 2023.

[20] Fritz, T. M., Eastham, S. D., Speth, R. L., and Xu, M., "Aircraft Plume Chemistry, Emissions, and Microphysics Model," GitHub, April 2020. https://doi.org/10.5281/zenodo.3755701, URL https://github.com/MIT-LAE/APCEMM, accessed on July 22, 2023.

[21] Kärcher, B., "A trajectory box model for aircraft exhaust plumes," *Journal of Geophysical Research: Atmospheres*, Vol. 100, No. D9, 1995, pp. 18835–18844. https://doi.org/10.1029/95JD01638.

[22] Hosder, S., Walters, R., and Perez, R., "A Non-Intrusive Polynomial Chaos Method For Uncertainty Propagation in CFD Simulations," *44th AIAA Aerospace Sciences Meeting and Exhibit*, 2006. https://doi.org/10.2514/6.2006-891.

[23] Feinberg, J., Eck, V. G., and Langtangen, H. P., "Multivariate Polynomial Chaos Expansions with Dependent Variables," *SIAM Journal on Scientific Computing*, Vol. 40, No. 1, 2018, pp. A199–A223. https://doi.org/10.1137/15M1020447.

[24] Xiu, D., Karniadakis, G. E., and Comput, S. J. S., "The Wiener-Askey Polynomial Chaos for Sochastic Differential Equations," *Society for Industrial and Applied Mathematics*, Vol. 24, 2002, pp. 619–644. https://doi.org/10.1137/S1064827501387826.

[25] Feinberg, J., "chaospy," GitHub, 2023. URL https://github.com/jonathf/chaospy, accessed on May 21, 2023.

[26] Feinberg, J., and Langtangen, H. P., "Chaospy: An open source tool for designing methods of uncertainty quantification," *Journal of Computational Science*, Vol. 11, 2015, pp. 46–57. https://doi.org/10.1016/j.jocs.2015.08.008.

[27] Feinberg, J., and Langtangen, H. P., "Generalized polynomial chaos," chaospy, No year. URL https://chaospy.readthedocs.io/en/master/user_guide/advanced_topics/generalized_polynomial_chaos.html, accessed on Nov 23, 2023.

[28] Teoh, R., Schumann, U., Majumdar, A., and Stettler, M. E. J., "Mitigating the Climate Forcing of Aircraft Contrails by Small-Scale Diversions and Technology Adoption," *Environmental Science & Technology*, Vol. 54, No. 5, 2020, pp. 2941–2950. https://doi.org/10.1021/acs.est.9b05608.

[29] Elmourad, J. A., "Evaluating Fuel-Climate Tradeoffs in Contrail Avoidance," Master's thesis, Massachusetts Institute of Technology, 2023. URL https://dspace.mit.edu/handle/1721.1/150282, accessed on August 9, 2023.